Microchimica Acta (2023) 190:52
https://doi.org/10.1007/s00604-022-05624-8

ORIGINAL PAPER

$Ti_3C_2@Bi_2O_3$ nanoaccordion for electrochemical determination of miRNA-21

Ruizhuo Ouyang[1,2] · Lan Jiang[1,2] · Xianjin Xie[1,2] · Ping Yuan[3] · Yuefeng Zhao[1,2] · Yuhao Li[1,2] · Abel Ibrahim Balbín Tamayo[2,4] · Baolin Liu[2,5] · Yuqing Miao[1,2]

Received: 21 July 2022 / Accepted: 15 December 2022 / Published online: 14 January 2023

Abstract

Based on a dual signal amplification strategy of novel accordion-like Bi_2O_3-decorated Ti_3C_2 ($Ti_3C_2@Bi_2O_3$) nanocomposites and hybridization chain reaction (HCR), an ultra-sensitive electrochemical biosensor was constructed for miRNA-21 detection. By etching Ti_3AlC_2 with HF, Ti_3C_2 with an accordion-like structure was first obtained and subsequently covered by Bi_2O_3 nanoparticles (NPs), forming $Ti_3C_2@Bi_2O_3$. A layer of Au NPs was electrodeposited on the glassy carbon electrode coated with $Ti_3C_2@Bi_2O_3$, which not only significantly improved the electron transport capacity of the electrode but also greatly increased its surface active area. Upon the immobilization of the thiolated capture probe (SH-CP) on the electrode, the target miRNA-21 specifically hybridized with SH-CP and thus opened its hairpin structure, triggering HCR to form a long double strand with the primers H1 and H2. A large number of the electrochemical indicator molecules were thus embedded inside the long double strands to produce the desirable electrochemical signal at a potential of − 0.19 V (vs. Ag/AgCl). Such dual signal amplification strategy successfully endowed the biosensor with ultra-high sensitivity for miRNA-21 detection in a wide linear range from 1 fM to 100 pM with a detection limit as low as 0.16 fM. The excellent detection of miRNA-21 in human blood plasma displayed a broad prospect in clinical diagnosis.

Keywords Electrochemical biosensor · Differential pulse voltammetry · MiRNA-21 · $Ti_3C_2@Bi_2O_3$ · HCR

Introduction

MicroRNAS (miRNAs) are small, non-encoded RNA sequences and typically consist of 18 to 25 nucleotides [1, 2], which play a vital role in biological processes and gene expression [3], such as cellular development, differentiation, proliferation, and metabolism. As one of target miRNAs, whose concentration is of interest [4], miRNA-21 with 22–23 nucleotides in length is chosen [5]. The dysregulation of miRNA-21 is essential in various cancer types such as lung cancer [6], gastric cancer, breast cancer, and colorectal cancer [7]. However, it is extremely difficult to detect miRNAs in real samples due to their short sequences, low abundance, relatively low expression levels, and highly similar sequence between family members [8]. Therefore, there is an urgent need to develop an ultra-sensitive miRNA detection method for clinical diagnosis [9]. The traditional analytical techniques, including Northern blot [10], microarrays [11], and real-time quantitative polymerase chain reaction (RT-qPCR) [12], have shown satisfactory performance for the miRNA detection, but their shortcomings like high

Ruizhuo Ouyang, Lan Jiang, Xianjin Xie, and Ping Yuan contributed to this work equally as co-first authors.

✉ Ruizhuo Ouyang
ouyangrz@usst.edu.cn

Abel Ibrahim Balbín Tamayo
ibrahim@fq.uh.cu

Baolin Liu
blliuk@usst.edu.cn

Yuqing Miao
yqmiao@usst.edu.cn

1 Institute of Bismuth and Rhenium Science, School of Materials and Chemistry, University of Shanghai for Science and Technology, Shanghai 200093, China

2 USST-UH International Joint Laboratory for Tumor Diagnosis and Energy Treatment, University of Shanghai for Science and Technology, Shanghai, China

3 Department of Cardiopulmonary Circulation, School of Medicine, Shanghai Pulmonary Hospital, Tongji University, Shanghai 200433, China

4 Faculty of Chemistry, University of Havana, 10400 Havana, Cuba

5 School of Health Science and Engineering, University of Shanghai for Science and Technology, Shanghai 200093, China

cost, complex operation, and large sample consumption still hinder their further development. In order to overcome these limitations, more and more innovative methods have been developed, like fluorescence [13], electrochemiluminescence (ECL) [14], colorimetry [15], surface plasmon resonance [16], and electrochemical sensor. Among them, the electrochemical sensing technique has ignited greater interest due to its advantages of handy operation, excellent selectivity, rapidness, and low cost [17, 18]. The amplification of electrochemical signals using various nanomaterials is extensively utilized to increase the diagnostic sensitivity of electrochemical biosensors [19–22]

For example, the p-Co-BDC/AuNPs-based multiplex signal amplification was reported for ultra-sensitive electrochemical determination of miRNAs [23] and a versatile non-enzymatic electrochemical biosensor was developed by integrating a molecular beacon-like catalytic hairpin assembly circuit with MOF@Au@G-triplex/hemin nanozyme to ultra-sensitively detect miR-721 [24]. In order to improve the sensitivity and accuracy for the target miRNA measurement, a number of signal amplification strategies have been evolved on the basis of nanomaterials and biological technologies [25, 26]. Nanomaterials usually make major contribution to improving the electrode's performance by providing adequate active sites. MXene is a family of two-dimensional (2D) transition metal carbide/nitride materials that have currently being extensively studied and attract an increasing interest due to their excellent versatile properties [27]. Titanium carbide (Ti_3C_2), as a member of the MXene's family, is characteristic of simple preparation, unique structure, and rich active sites and shows great potential in fabricating electrochemical biosensors to detect various biomolecules [28]. Ti_3C_2 may obtain a layered structure with large surface area and active sites through etching with hydrofluoric acid (HF), which can significantly improves its electrochemical performance, but both the surface area and the active sites will be further decreased because of the formation of hydrogen bonds from the introduced surface functional groups like -F, –OH, and = O during the preparation and the van der Waals interactions between layers, causing re-stacking and aggregation [29].Therefore, it is fairly necessary to produce Ti_3C_2-based composites with improved properties through functionalization so as to enhance the electrochemical performance of sensor. Bi_2O_3 is quite promising as electrochemical sensing material due to its good stability, extremely low toxicity, preferable biocompatibility, and favorable electrical properties, especially for the detection of biomolecules [30]. The heterostructures are believed to combine the advantages of each 2D material and thus exert better properties to the composite due to the synergistic effects [31].

Herein, the heterogeneous $Ti_3C_2@Bi_2O_3$ nanocomposites were produced with an accordion-like structure to amplify the signal together with the HCR amplification strategy for the purpose to construct an ultra-sensitive and stable electrochemical sensor towards miRNA-21 detection [32–35]. Methylene blue (MB) was selected as an electroactive indicator for the differential pulse voltammetry (DPV) measurements [36, 37]. As shown in Scheme 1, taking the advantages of good conductivity and numerous active sites exposed outside the as-prepared $Ti_3C_2@Bi_2O_3$ composites, the proposed electrochemical sensor received greatly improved electrochemical properties for miRNA-21 detection. Based on the excellent dual amplification strategy from both $Ti_3C_2@Bi_2O_3$ and HCR, admirable analytical performances were finally achieved including fast response, ultrahigh sensitivity, superior stability, excellent specificity, and good reproducibility. A promising bismuth-based electrochemical sensing platform was thus created showing new insights and great potential for the ultra-sensitive detection of miRNAs in future clinical diagnosis and treatment of diseases.

Experimental

Materials and apparatus

Titanium aluminum carbide (Ti_3AlC_2) powder was purchased from Haoxi Nanotechnology Co., Ltd. (Shanghai, China). 6-Mercaptohexanol (MCH), tris(carboxyethyl) phosphine (TCEP), potassium chloride (KCl), Methylene blue (MB), hydrogen tetrachloroaurate trihydrate ($HAuCl_4{\cdot}3H_2O$), diethyl pyrocarbonate (DEPC) water, potassium hexacyanoferrate-III ($K_3[Fe(CN)_6]$), potassium hexacyanoferrate-II ($K_4[Fe(CN)_6]$), HF, sodium sulfate (Na_2SO_4), ammonia solution (NH_4OH), bismuth nitrate pentahydrate ($Bi(NO_3)_3{\cdot}5H_2O$), and phosphate buffer solution (PBS) were all purchased from Shanghai Titan Technology Co., Ltd. All chemical reagents were of analytical grade and used as received without any further purification. All the oligonucleotides were synthesized by Nanjing Kingsray Biotechnology Co., Ltd. (Nanjing, China) and purified by high-performance liquid chromatography. The detail nucleotides sequences were summarized in Table S1.

All electrochemical measurements were carried out on the electrochemical workstation (AUTOLAB-PGSTAT302N, Metrohm China Co., Ltd.) with the conventional three-electrode system applied, where the glassy carbon electrode (GCE), the Ag/AgCl electrode, and the platinum wire were used as the working electrode, the reference electrode, and the counter electrode, respectively. The chemical elements and morphologies of the materials were observed by the energy dispersive spectroscopy (EDS) and the scanning electron microscope (SEM) (JSM-6701F, JEOL Co, Ltd.). The crystal structures of the materials were characterized

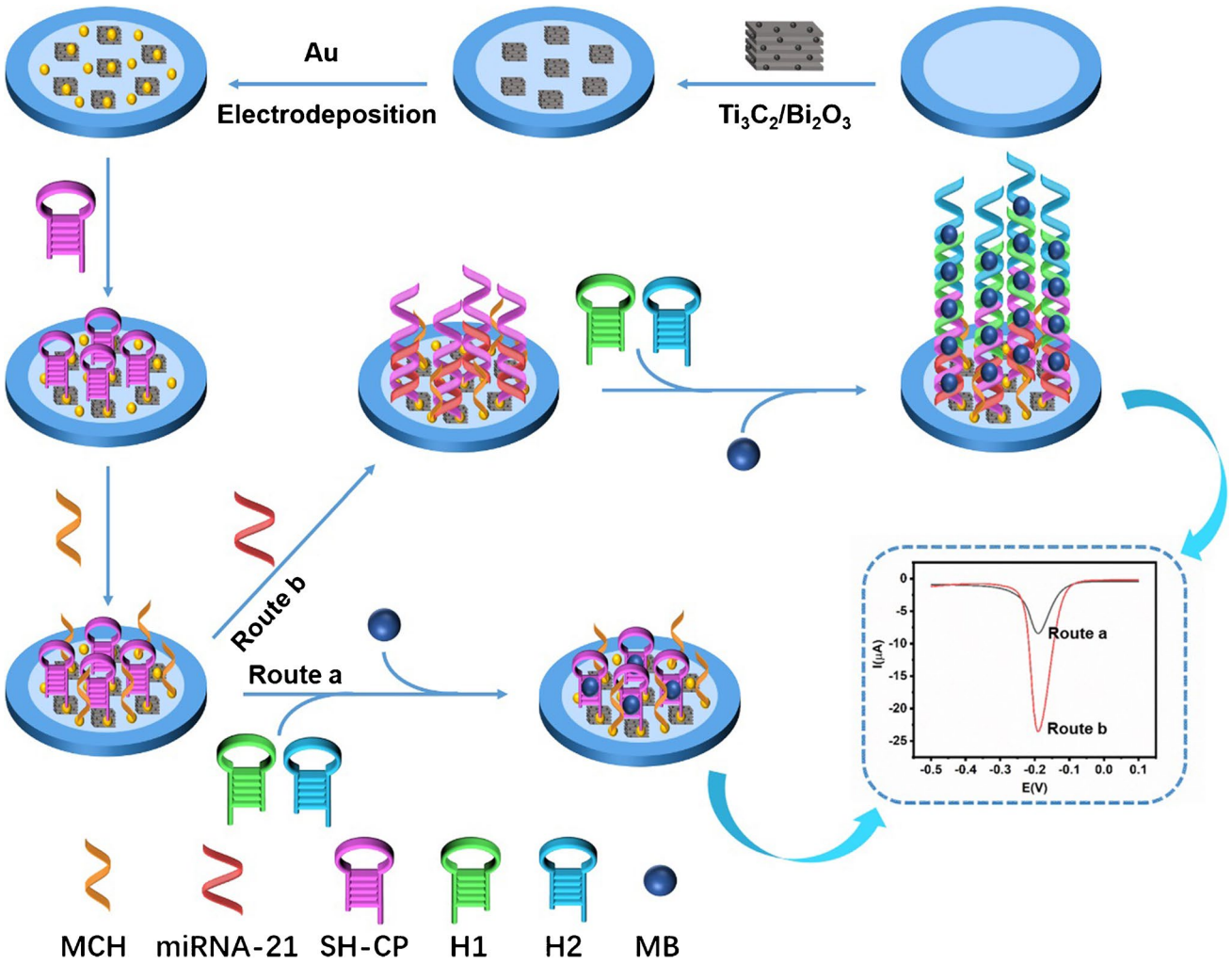

Scheme 1 The schematic preparation of the proposed electrochemical miRNA sensor based on the double amplification strategy of the accordion-like $Ti_3C_2@Bi_2O_3$ nanocomposites and HCR, and the working principle for the ultra-sensitive detection of miRNA-21

by X-ray diffraction (XRD, Smartlab-3, Rigaku, USA). The static water contact angle (CA) measurements were carried out using a DSA25 goniometer (KRÜSS GmbH, Germany). Agarose gel electrophoresis was carried out using the DYCZ-24F electrophoretic device (Beijing Liuyi, China) and imaged via a Tanon-3500 gelimage system (Shanghai, China). RT-qPCR was performed and analyzed on a StepOne instrument (ABI, Foster, CA, USA).

Preparation of accordion-like $Ti_3C_2@Bi_2O_3$ nanocomposites

Ti_3AlC_2 was first etched by HF to obtain the accordion-like Ti_3C_2. Briefly, 1.0 g of Ti_3AlC_2 powder was placed in 30 mL HF solution (49 wt%) which was mixed thoroughly followed by continuous stirring for 48 h at 35 °C. Then, the mixed solution was repeatedly washed with deionized water until the pH was close to neutral value, forming theTi_3C_2 with accordion-like structure. The product was finally collected and dried at 80 °C under vacuum for 8 h.

The heterogeneous $Ti_3C_2@Bi_2O_3$ nanocomposites were prepared by the hydrothermal method. First, 150 mg of Ti_3C_2 powder was added into 20 mL deionized water which was stirred for 30 min until the powder uniformly dispersed. Then, 90 mg $Bi(NO_3)_3{\cdot}5H_2O$ was dissolved in the above solution followed by a 30-min stirring. The mixture was then transferred to a 50 mL polytetrafluoroethylene-lined stainless-steel autoclave after its pH was adjusted to 8.0 with NH_4OH. The reaction was kept at 180 °C for 12 h. Finally, the $Ti_3C_2@Bi_2O_3$ nanocomposites with the desired heterostructure were obtained by successively centrifuging with ultrapure water and absolute ethanol, and dried under vacuum at 80 °C for 8 h.

Fabrication of the Ti_3C_2@Bi_2O_3-based electrochemical biosensor

Before the electrode modification, the bare GCE was well polished with 0.3 and 0.05 μm alumina slurry, respectively. Then, 6 μL Ti_3C_2@Bi_2O_3 suspension (1.0 mg/mL) was first dropped onto the pretreated GCE (Ti_3C_2@Bi_2O_3/GCE) which was dried at 35 °C. Afterwards, the Ti_3C_2@Bi_2O_3/GCE was immersed into 1.0 mM $HAuCl_4$ solution containing 0.01 M Na_2SO_4 so as to allow Au nanoparticles (NPs) being electrodeposited on the electrode surface (Au/Ti_3C_2@Bi_2O_3/GCE) under − 0.2 V for 300 s via the chronoamperometry, where Au NPs were extensively used to immobilize biomolecules through forming stable bonds between Au and S or N [38]. Then, 6 μL of 1 μM thiolated capture probes (SH-CP) was directly pipetted onto the surface of Au/Ti_3C_2@Bi_2O_3/GCE on which the incubation lasted for 6 h at room temperature to form Au–S bond. The above electrode was subsequently sealed with 1 mM MCH solution for 1 h and incubated with 6 μL miRNA-21 solutions of different concentrations for 2 h at room temperature. 6 μL of a mixed solution containing H1 (0.5 μM) and H2 (0.5 μM) was then dropped on the surface of the obtained electrode followed by the incubation at room temperature for 2 h. Finally, 6 μL of 1 mM MB solution was incubated with the above obtained electrode at room temperature for 1 h to serve as an electron mediator, producing the detectable electrochemical signal for the miRNA-21 detection.

DPV measurements of miRNA-21

DPV measurements of miRNA-21 was examined with the proposed miRNA biosensor in 0.1 M PBS (pH 7.4), where the scanning potential ranged from − 0.5 to 0.1 V with the pulse amplitude and the pulse set as 0.07 V and 0.05 s, respectively. The peak responses to MB were recorded at − 0.19 V (*vs.* Ag/AgCl) to quantify the target miRNA-21 at different concentrations. The measurements were generally repeated under the same experimental conditions for three times.

Analysis of human blood samples

Firstly, 1 mL healthy human serum provided by Changhai Hospital, Naval Medical University (Shanghai, China) was first diluted by tenfold with 0.01 M PBS (pH 7.4) and standard addition of miRNA-21 was applied to obtain blood samples containing different levels of miRNA-21 (10 fM, 10 pM, and 100 pM). Here, the blood samples were stabilized with elhylene diamine tetraacetic acid (EDTA). 6 μL of the diluted healthy human serum containing various concentrations of miRNA-21 were separately incubated with the proposed biosensor. Afterwards, the DPV responses to MB at − 0.19 V (*vs.* Ag/AgCl) were recorded to quantify miRNA-21 in the blood samples. In general, the measurements were repeated under the same experimental conditions for three times to ensure the accuracy and precision of the detection.

QRT-PCR analysis

RNA samples were converted to cDNA using the Revert Aid Premium Reverse Transcriptase Reverse Transcription Kit (Thermo) according to the manufacturer's instructions. The minimum amount of the extracted total RAN required to detect the target RNA is approximately 46 ng. The reaction conditions were set as follows: the reaction was successively kept for 10 min at 20 °C and 30 min at 50 °C for reverse transcription, and continued at 85 °C for 5 min before being ended. Finally, the cDNA samples were stored at − 20 °C for further analysis by qRT-PCR. PCR assays were performed on a StepOnePlus RT-PCR instrument using the Fast qPCR Master Mix kit. The reaction system was first incubated at 95 °C for 3 min, followed by 40 cycles at 95 °C for 5 s and 60 °C for 30 s, respectively.

Results and discussion

Working principle of the proposed miRNA sensor

As illustrated in Scheme 1, the proposed electrochemical miRNA sensor was prepared based on the double amplification strategy of the accordion-like Ti_3C_2@Bi_2O_3 nanocomposites and HCR for the ultra-sensitive miRNA-21 detection. Firstly, the Ti_3C_2@Bi_2O_3 composites were immobilized on the surface of a bare GCE through electrostatic interaction and van der Waals force (Ti_3C_2@Bi_2O_3/GCE), which was advantageous of higher specific surface area, better conductivity, and more active sites due to unique accordion-like structure Ti_3C_2 of and the modification of Bi_2O_3 NPs. Secondly, Au/Ti_3C_2@Bi_2O_3/GCE was obtained by forming Au NPs on the surface of Ti_3C_2@Bi_2O_3/GCE via electrodeposition at − 0.2 V for 300 s in order to improve the electrochemical signal, reduce the Rp, and provide Au atoms to form Au–S bonds with -SH inside the capture probe. After the immobilization of the stem-loop structure SH-CP on the surface of Au/Ti_3C_2@Bi_2O_3/GCE, MCH was used to cover the unreacted Au sites and eliminate the nonspecific adsorption on the electrode surface. Apparently, in route a, without target miRNA-21, the HCR process will not be further triggered by H1 and H2 because the hairpin structure of SH-CP cannot be opened. MB can be embedded in dsDNA through π–π stacking interactions; thus, only a small amount of MB can be embedded in the hairpin structure of SH-CP without miRNA-21, resulting in a rather weak DPV signal. In route

b, while in the absence of the target miRNA-21, the hairpin structure can be opened due to specific hybridization with SH-CP, leading to the opening of H1. Similarly, the opened H1 as an elicitor subsequently opens H2, and the open H2 initiates the opening of H1 in turn. As a result, the HCR process is triggered, forming the long double strand used to capture MB.

An appropriate electrochemical signal indicator is very important to develop an electrochemical sensing platform with ultra-sensitivity. MB as a signal indicator can be stably bound to the double-stranded nucleic acid sequences through the interaction of π-π conjugated electrons and hydrogen bonds, while shows relatively poorer binding ability with the single-stranded DNA, as the enhanced binding of double-stranded DNA intercalation exerts double-stranded DNA better affinity with MB. As a result, MB would accumulate in large quantities on the electrode surface via hydrogen bonding and static electricity. Here, SH-CP highly matched the target miRNA-21 sequence, in contrast, the presence of low concentrations of miRNA-21 or sequence mismatched RNA could reduce the amount of MB bound to the dsDNA through intercalation, resulting in effectively improved specificity of the biosensor. In the potential range from − 0.5 V to 0.1 V, MB showed significant and amplified DPV signal correlated to the concentration of the target miRNA-21 based on the following redox reaction (Scheme 2).

Compared with traditional methods without any signal amplification strategy [17, 39], the sensitivity of the designed electrochemical miRNA sensor could be significantly improved based on the dual signal amplification strategy by combining the accordion-like Ti_3C_2@Bi_2O_3 composites with HCR.

Characterizations of the Ti_3C_2@Bi_2O_3 composites

The accordion-like structures of both Ti_3C_2 and Ti_3C_2@Bi_2O_3 were confirmed by SEM images (Fig. 1A and B). Figure 1B shows that Bi_2O_3 NPs fully and uniformly grew

Scheme 2 The redox reaction of MB on the electrode surface

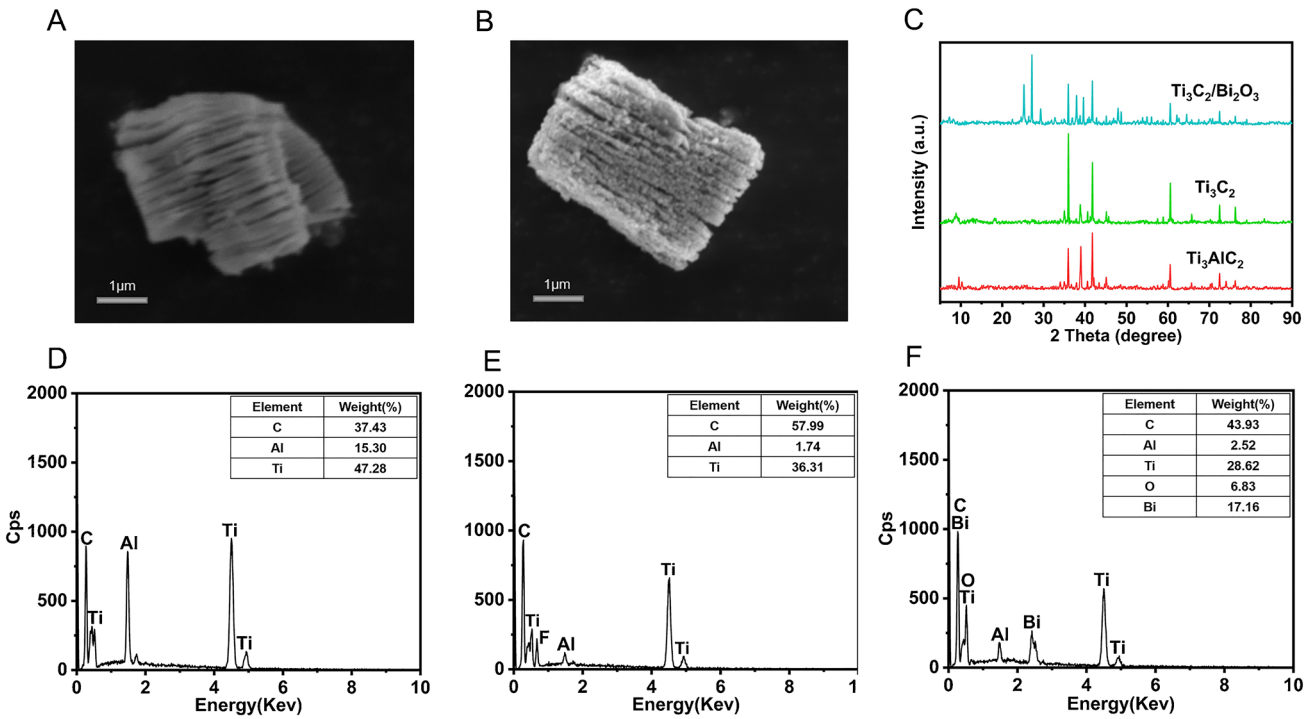

Fig. 1 SEM images of (**A**) Ti_3C_2 and (**B**) Ti_3C_2@Bi_2O_3 and (**C**) XRD of Ti_3AlC_2, Ti_3C_2, and Ti_3C_2@Bi_2O_3. EDS of (**D**) Ti_3AlC_2, (**E**) Ti_3C_2, and (**F**) Ti_3C_2@Bi_2O_3

on the surface of the layered Ti_3C_2 (Fig. 1A) without changing the layer structure obviously, forming the accordion-like Ti_3C_2@Bi_2O_3 nanocomposites, which endowed the structure larger specific surface area and Ti_3C_2@Bi_2O_3 better conductivity than each single material, developing a unique micro-nano heterostructure to increase the electron migration rate. Thus, the interwoven and interconnected Bi_2O_3 NPs grew evenly onto exterior of Ti_3C_2, maintaining the original layered structure of Ti_3C_2, increasing the reactive area, and confining the probes and targets together to increase the chance of collision and improve the efficiency of hybridization. Such an accordion-like micro-nano heterostructure is fairly preferred to develop sensor with improved sensitivity. As shown in Fig. 1C, the strong XRD peak of Ti_3AlC_2 at 38° was obviously weakened (green) since a large amount of Al was etched away. Several additional strong peaks clearly observed in the XRD spectrum of the Ti_3C_2@Bi_2O_3 composites verified the presence of Bi_2O_3 (blue), further providing evidence that the Ti_3C_2@Bi_2O_3 composites was successfully synthesized. Moreover, the significant reduction in the proportion of Al from 15.30 (Fig. 1D) to 1.74% (Fig. 1E) revealed the successful etching away of Al from Ti_3AlC_2, and the presence of O and Bi by 6.83% and 17.16% in Fig. 1F further proved the successful synthesis of the Ti_3C_2@Bi_2O_3 composites.

In order to explore the biocompatibility of the Ti_3C_2@Bi_2O_3 composites, the 4T1 breast cancer cells were selected to evaluate their toxicity using the CCK8 assay (Fig. 2A). Clearly, in the concentration range of Ti_3C_2@Bi_2O_3 from 6.25 to 200 μg/mL, the cells maintained a good survival rate with a slight decrease, even at the concentration as high as 200 μ g/mL, 90% of the cells were still capable of surviving, revealing the extremely low toxicity of the as-prepared Ti_3C_2@Bi_2O_3 nanocomposites. The favorable hydrophily of Ti_3C_2@Bi_2O_3 was confirmed by their significantly lower contact angle (Fig. 2B, b) than that of the bare electrode (Fig. 2B, a). The electrodeposition of Au NPs on the surface of Ti_3C_2@Bi_2O_3/GCE further improved the better hydrophilicity of Au/Ti_3C_2@Bi_2O_3/GCE by reducing contact angle to 34° (Fig. 2B, c). While the immobilization of biomolecules to the electrode did not significantly change the contact angle (Fig. 2B, d). All the results indicate that the as-prepared Ti_3C_2@Bi_2O_3 nanocomposites were characteristic of low toxicity and good hydrophilicity, which provide desirable support for the application of the biosensor in the analysis of actual samples.

Electrochemical properties of the biosensing platform

The interface properties of the stepwise modified electrode were analyzed by both CV and EIS, respectively. A pair of clearly defined quasi-reversible redox peaks of $[Fe(CN)_6]^{3-/4-}$ were observed for the bare GCE (Fig. 3A, curve a), which remarkably increased when the Ti_3C_2@Bi_2O_3 composites were modified (Fig. 3A, curve b), much higher than that of either Ti_3C_2 (Fig. 3A, curve h) or Bi_2O_3 (Fig. 3A, curve i), confirming the effectively promoted electron transfer over the electrode surface by Ti_3C_2@Bi_2O_3. The continuously increasing redox peaks were obtained with Au/Ti_3C_2@Bi_2O_3/GCE (Fig. 3A, curve c), resulting from the excellent electrical conductivity of Au NPs and the large active surface of Ti_3C_2@Bi_2O_3 which allowed more Au NPs deposited on. As expected, the sequential immobilization of biomolecules of SH-CP, MCH, and miRNA-21 on Au/Ti_3C_2@Bi_2O_3/GCE (Fig. 3A, curves d–f) caused continuous decrease of peak currents due to the electrostatic repulsion interaction, the filling of the unreacted Au sites and the specific hybridization with SH-CP which hindered the transfer of electrons on the electrode surface. Although the occurrence of HCR and the formation of longer dsDNA on the electrode surface further inhibited the diffusion of ferricyanide to the electrode surface when the mixture of H1 and H2 was added, the peak current was still high enough for the target detection (Fig. 3A, curve g).

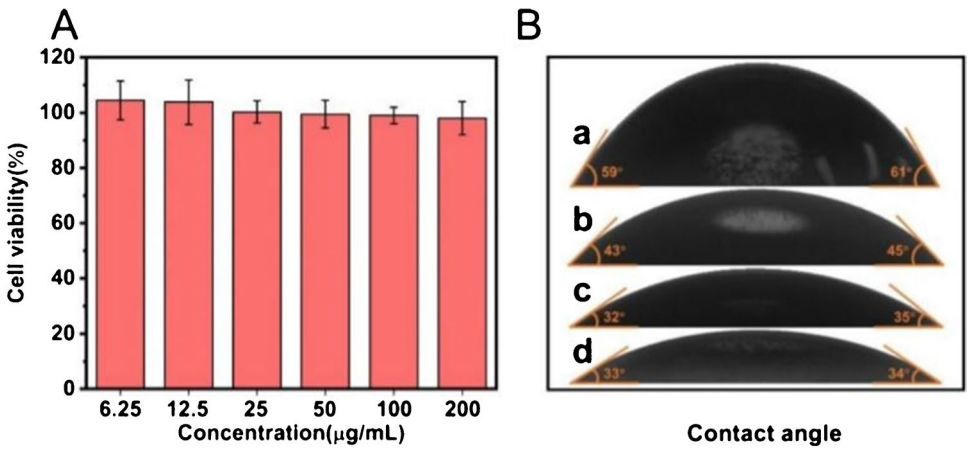

Fig. 2 (**A**) Relative survival rate of 4T1 breast cancer cells at different concentrations of Ti_3C_2@Bi_2O_3, error bar = RSD (n = 3). (**B**) CA measurements of (a) GCE, and GCEs modified with (b) Ti_3C_2@Bi_2O_3, (c) Au/Ti_3C_2@Bi_2O_3, and (d) H1,H2/miRNA-21/MCH/SH-CP/Au/Ti_3C_2@Bi_2O_3, respectively

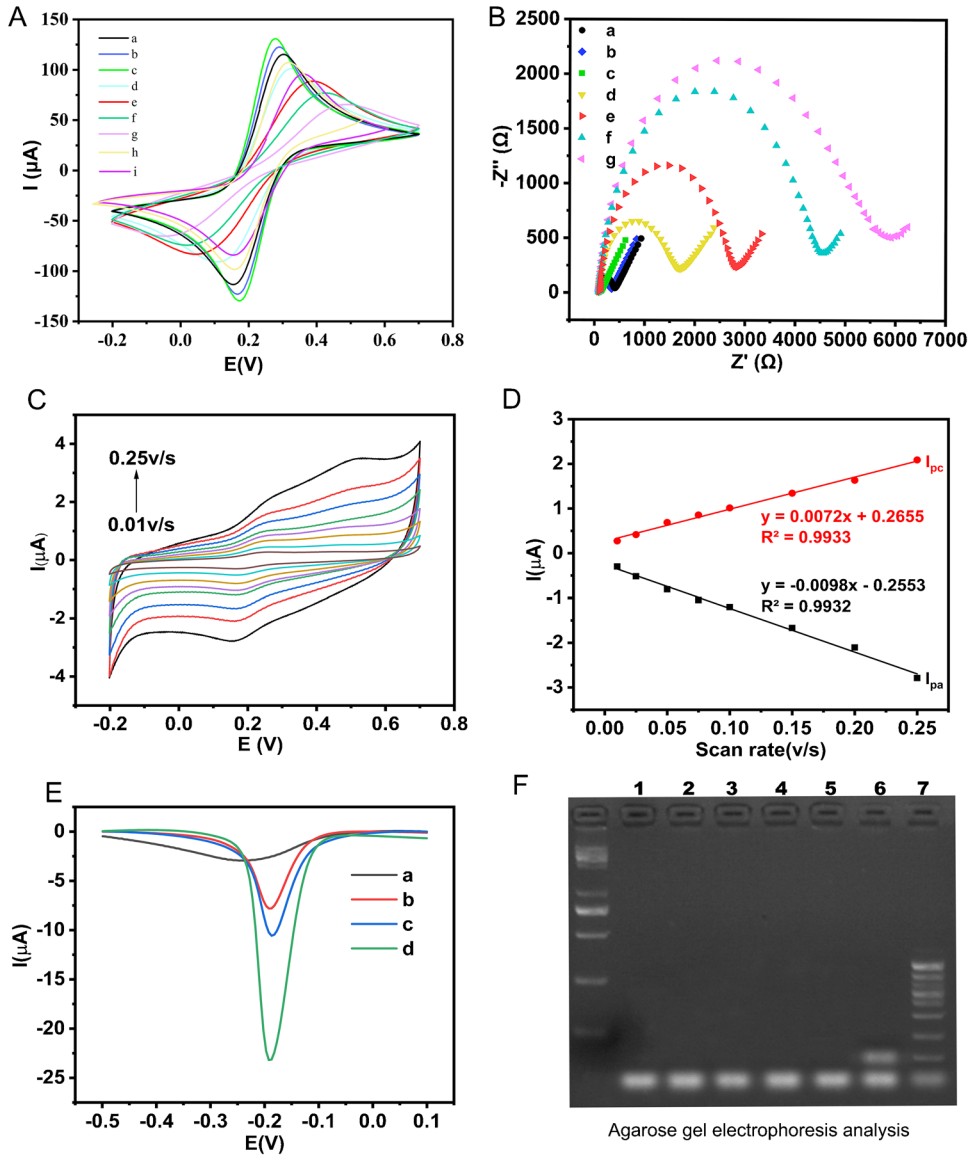

Agarose gel electrophoresis analysis

Fig. 3 (**A**) CV curves scanned from − 0.2 V to 0.7 V (*vs.* Ag/AgCl) at a scan rate of 0.1 V/s and (**B**) EIS curves (inset: the equivalent electrical circuit) recorded from 0.1 to 10^5 Hz in 5.0 mM $[Fe(CN)_6]^{3-/4-}$ solution containing 0.1 M KCl: (a) bare GCE, (b) Ti_3C_2@Bi_2O_3/GCE, (c) Au/Ti_3C_2@Bi_2O_3/GCE, (d) SH-CP/Au/Ti_3C_2@Bi_2O_3/GCE, (e) MCH/SH-CP/Au/Ti_3C_2@Bi_2O_3/GCE, (f) miRNA-21/MCH/SH-CP/Au/Ti_3C_2@Bi_2O_3/GCE, (g) H1,H2/miRNA-21/MCH/SH-CP/Au/Ti_3C_2@Bi_2O_3/GCE, (h) Ti_3C_2/GCE, and (i) Bi_2O_3/GCE. (**C**) CV curves obtained in 5.0 mM $[Fe(CN)_6]^{3-/4-}$ solution containing 0.1 M KCl with H1, H2/miRNA-21/MCH/SH-CP/Au/Ti_3C_2@Bi_2O_3-modified GCE at different scan rates from 0.01 to 0.25 V/s. (**D**) Plots of CV peak currents *versus* scan rate. (**E**) DPV measurements with the differently modified electrodes at various conditions in 0.1 M PBS (pH 7.4): (a) MB/Au/Ti_3C_2@Bi_2O_3/GCE, (b) MB/SH-CP/Au/Ti_3C_2/Bi_2O_3/GCE, (c) MB/miRNA-21/MCH/SH-CP/Au/Ti_3C_2@Bi_2O_3/GCE, and (d) MB/H1,H2/miRNA-21/MCH/SH-CP/Au/Ti_3C_2@Bi_2O_3/GCE. (**F**) Agarose gel electrophoresis analysis with lanes from left to right: (1) SH-CP, (2) miRNA-21, (3) H1, (4) H2, (5) SH-CP + H1 + H2, (6) SH-CP + miRNA-21, and (7) SH-CP + miRNA-21 + H1 + H2

The interface reaction resistance (Rp) is attributed to the semicircular part of the typical EIS at the higher frequency which represents the electron transfer from the electroactive probe to the electrode surface. The increase in the diameter of the semicircular part indicates an increase in the Rp value of the interface. The fitted EIS equivalent circuit was shown in the upper right of Fig. 3B, where Rs is mainly the resistance of the electrolyte solution, Rp the interface reaction resistance, *W* the Warburg impedance related to the diffusion of ions in the bulk electrode, and CPE the interface capacitance. Using $[Fe(CN)_6]^{3-/4-}$ as redox probe, the bare GCE showed a very small semicircle (Fig. 3B, curve a), while the semicircle diameter gradually decreased for Ti_3C_2@Bi_2O_3 and Au/Ti_3C_2@Bi_2O_3/GCE. (Fig. 3B, curves b and c). After SH-CP, MCH, miRNA-21, H1, and H2 were assembled on the electrode surface in sequence, the diameter of the semicircle gradually increased (Fig. 3B, curves d–g) owing to the continuous accumulation of biomolecules on the electrode surface. The obtained EIS results were in good accordance with that of CV, indicating the successful construction of the electrochemical miRNA-21 biosensor.

The electrochemical behavior of the electrode modified with H1, H2/miRNA-21/MCH/SH-CP/Au/Ti_3C_2@Bi_2O_3 was further evaluated by recording the CV curves at scan rates (v) ranging from 0.01 to 0.25 V/s (Fig. 3C). The redox peak current of $[Fe(CN)_6]^{3-/4-}$ increased with the increasing scan rate. Both the oxidation peak current (I_{pa}) and the reduction peak current (I_{pc}) were linearly related with the scan rate (Fig. 3D). Two fitted linear equations were obtained as I_{pa} (μA) = 0.2655 + 0.0072 v (V/s) with a correlation coefficient (R^2) of 0.9933) and I_{pc} (μA) = − 0.2553 − 0.0098 v

(V/s) ($R^2 = 0.9932$), respectively, indicative of a typical adsorption control process over the electrode surface.

The feasibility of the proposed miRNA biosensor was examined by DPV in 0.1 M PBS, as shown in Fig. 3E, where the scanning potential ranged from − 0.5 to 0.1 V with the pulse amplitude and the pulse set as 0.07 V and 0.05 s, respectively. When the electrode was modified with Au/Ti_3C_2@Bi_2O_3, almost no current signal was generated with the DPV curve close to a horizontal line (curve a, Fig. 3E), indicating the failure to immobilize MB onto the electrode surface. While the subsequent modification of SH-CP on Au/Ti_3C_2@Bi_2O_3/GCE led to the production of a weak peak current at -0.19 V (*vs* Ag/AgCl) as a small amount of MB was bound to the SH-CP (curve b, Fig. 3E). In the presence of miRNA-21, the DPV signal of MB kept increasing since more MB molecules were attached to the dsDNA resulting from the hybridization of miRNA-21 with SH-CP (curve c, Fig. 3E). Finally, the DPV signal increased significantly to the highest in the presence of H1 and H2, which was attributed to the embedment of large amount of MB inside the longer dsDNA as a result of the occurrence of HCR (curve d, Fig. 3E). These results demonstrates that the developed electrochemical sensor could be an ideal platform for the miRNA-21 detection. Furthermore, agarose gel electrophoresis analysis was performed on the molecular recognition events to confirm the feasibility of the constructed biosensor. In Fig. 3F, lanes 1–4 represented SH-CP, miRNA-21, H1, and H2, respectively. A clearly low molecular weight band could be observed. Lane 5 referred to the mixture of SH-CP, H1, and H2, which showed no new bands except for one band same as lanes 1–4, indicating the good metastability of the SH-CP, H1, and H2. No reaction occurred among their mixtures without miRNA-21. Lane 6 represented a mixture of miRNA-21, H1, and H2, in which a new band observed, revealing the successful hybridization of miRNA-21 with the SH-CP. The mixture of SH-CP, miRNA-21, and H1, H2 produced a band with significantly different electrophoretic mobilities (lane 7), which corresponded to the HCR products with various sizes. This proves that the HCR was successfully triggered in the presence of H1 and H2. These results further verified the good feasibility of the as-proposed method to detect miRNA-21.

All the experimental conditions were well optimized to achieve the best detection performance of the proposed electrochemical sensing platform (Fig. S1), whose analytical behavior was assessed toward different concentrations of miRNA-21 ranging from 1 fM to 100 pM. As shown in Fig. 4A, the peak current at − 0.19 V (*vs.* Ag/AgCl) gradually increased with the increase of miRNA-21 concentration because of the continuous accumulation of MB on the electrode surface. No current response was observed to the solution without miRNA-21, where the weak peak was likely caused by the non-specifically adsorbed MB. A good linear relationship was achieved between the peak current value (I_p) and the logarithm of miRNA-21 concentration (1og$c$) with a correlation equation of $I_p = -3.6951\log c - 65.691$ where the correlation coefficient of R^2 equaled 0.9977 (Fig. 4B), and the limit of detection (LOD) was calculated to be as low as 0.16 fM (S/N = 3), significantly lower than that of some previously reported sensors listed in Table 1. Here, LOD, expressed as the concentration, C_L, was derived from the smallest measure and X_L, $X_L = nX_{b1} + nS_{b1}$ ($n = 3$), where X_{b1} and S_{b1} refer to blank measures and standard deviation of the blank measures, respectively (more details were provided in the supporting materials).

RT-qPCR, as a classic nucleic acid detection method, has been widely applied in the fields of biomedical research and clinical analysis, where fluorescent groups are added to the PCR reaction system to monitor the entire PCR process in real time through the accumulation of fluorescent signals, and finally achieve the quantitative analysis of the unknown samples through the standard curve. Here, the RT-qPCR was employed to detect miRNA-21 for comparison (Fig. 4C). The cycle threshold (CT) value reaching the fluorescence threshold of 0.04 showed a good linearly growing trend within the concentration range from 100 fM to 100 nM. However, the fluorescence intensity did not reach the fluorescence threshold of 0.04 at the miRNA-21concentration higher than 100 nM, while the CT value only slightly increased as the concentration was less than 100 fM, revealing that both RT-qPCR and the developed sensor exhibited the same linear ranges. Moreover, the LOD in this work was significantly lower with a higher sensitivity. Besides, the other existing types of electrochemical miRNA sensors were also compared with the newly proposed sensor. As shown in Table 1, obvious advantages of superior detection limit and wider linear range were obtained for the miRNA-21 detection using this newly developed biosensor which was likely attributed to the excellent conductivity and extensively exposed active sites of Ti_3C_2@Bi_2O_3 as well as the stable and high amplification ability of HCR.

Selectivity, reproducibility, and stability

The analytical performance of the new biosensor was further evaluated with selectivity, stability and reproducibility as well. To assess the selectivity of the sensor, we selected three small nucleic acid molecules with different sequences from miRNA-21 as interferents. As can be seen in Fig. 4, the proposed sensor highly responded to the target miRNA-21 without interferents; however, no obvious response was observed with this sensor towards each of the interferents in the absence of the target miRNA-21. In the contrast, compared to the current response to single miRNA-21, the presence of each interferent, especially the S-RNA and T-RNA with 1 and 3 mismatched bases in sequences showing the

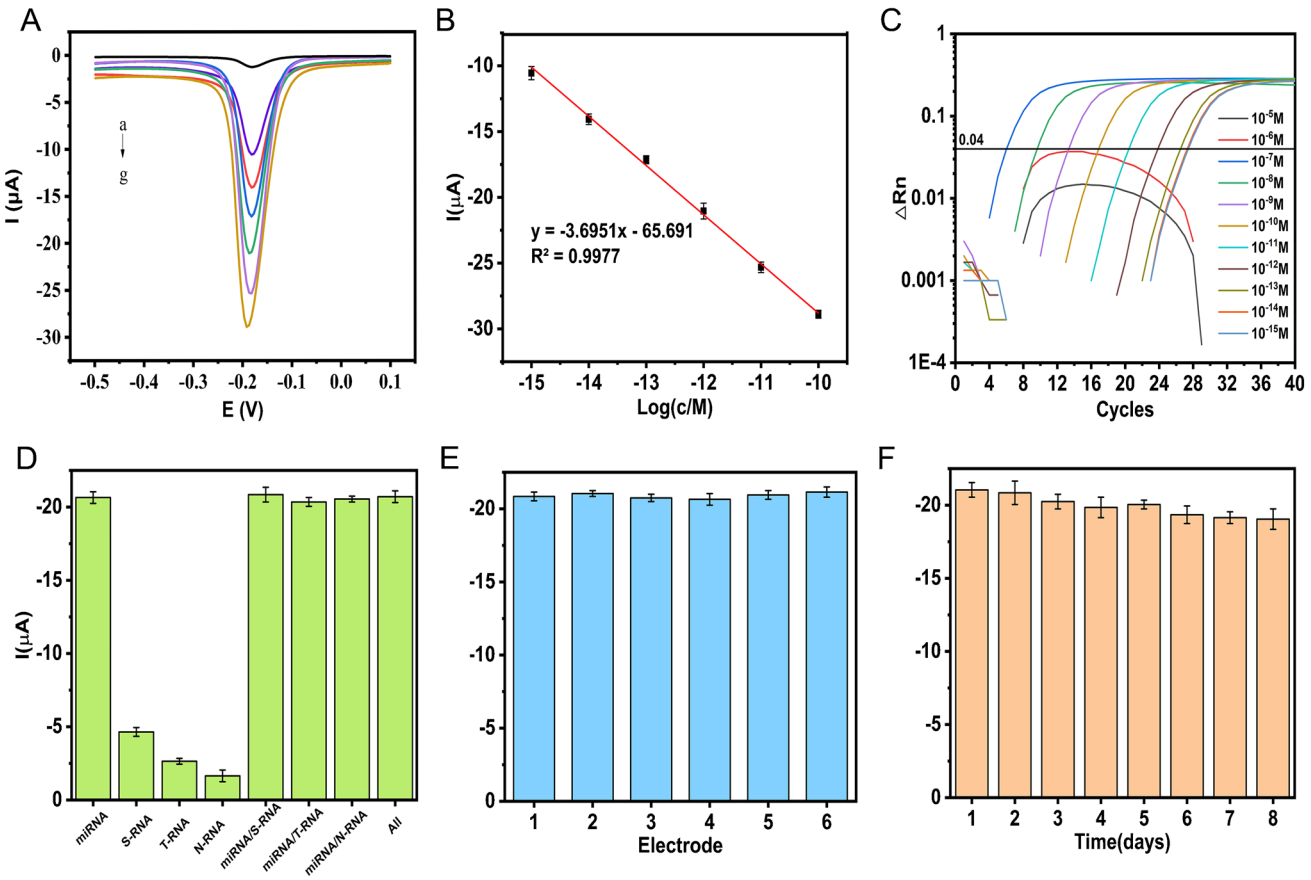

Fig. 4 (**A**) DPV responses of the newly developed electrochemical biosensor incubated with different concentrations of target miRNA-21 (a–g: 0 fM, 1 fM, 10 fM, 100 fM, 1 pM, 10 pM, and 100 pM). Potential range: − 0.5 V to + 0.1 V; amplitude, 0.07 V; pulse width, 0.05 s; pulse period, 0.2 s. (**B**) The calibration plot of I_p *vs.* log*c* obtained based on the DPV responses in the miRNA-21 concentration range from 1 fM to 100 pM. (**C**) The RT-qPCR curves obtained at different concentrations of miRNA-21. (**D**) The selectivity of the biosensor towards miRNA-21 in the coexistence of other miRNAs, where the error bars are standard deviations of three duplicate measurements. (**E**) The reproducibility and (**F**) stability of the biosensor for detection of miRNA-21 in pH 7.4 PBS. Error bar = RSD ($n = 3$)

Table 1 The analytical performances between the proposed biosensors and the previously reported ones for the detection of miRNAs

Sensors	MiRNA	Tech	Preparation (time/h)*	Response time/s	Application (time/min)*	Linear range	DOL	Refs
Au@MoS_2	miRNA-210	DPV	182	/	/	0.1 pM–10 nM	0.03 pM	[40]
HCR/EIM	miRNA-21	ASV	65	/	55	2.5 fM–25 nM	0. 12 fM	[41]
Au/PPy-rGO,	miRNA-16	DPV	30	/	155	10 fM–5 nM	1.57 fM	[42]
EATR/FC60	miRNA-141	DPV	46	/	/	0.1 pM–100 nM	7.78 fM	[43]
Tetrahedral DNA/G-Quadruplex – Hemin	miRNA-21	DPV	25	/	70	0.1 fM to 0.1 pM	0.04 fM	[44]
Fe_3O_4/CeO_2@Au	miRNA-21	DPV	64	/	/	1 fM–1 nM	0.33 fM	[24]
Cu-NMOF@Pt/HRP	miRNA-155	SWV	25	/	/	0.5 fM–0.1 nM	0.13 pM	[45]
Ti_3C_2@Bi_2O_3/HCR	miRNA-21	DPV	61	90	30	1 fM–100 pM	0.16 fM	This work

EIM, enzyme-induced metallization; *PPy-rGO*, polypyrrole-reduced graphene oxide; *FeCN*, iron-embedded nitrogen-rich carbon nanotubes; *EATR*, enzyme-assisted target recycling; *FC60*, fullerene NPs; Cu-NMOF@PtNPs/HRP, copper-based metal organic framework assembled by Pt NPs and horseradish peroxidase

*The time shown in the table were roughly assessed

high homology between members of the same miRNA family, did not clearly affect the current value of this sensor towards miRNA-21 indicating that the proposed sensing strategy is highly selective to miRNA-21. The sensor's good reproducibility was evidenced by detecting 1 pM miRNA-21 using six electrodes prepared separately (Fig. 4E), where a relative standard deviation (RSD) of 4.6% was achieved. The long-term storage stability was studied based on the daily measurements of the sensor stored at 4 °C within 8 days. The signal intensity still remained 85.3% of its initial current after 8 days (Fig. 4F), indicating the sensor's satisfactory stability.

Serum sample analysis

To assess the application potential of the newly developed biosensing platform, human serum samples were analyzed after being diluted tenfold with 0.01 M pH 7.4 PBS. Moreover, the standard addition of miRNA-21 was applied to detect the human serum samples, forming different miRNA-21concentrations of 10 fM, 10 pM, and 100 pM. Specifically, 6 μL of diluted serum containing various concentrations of miRNA-21 were incubated with the sensor, and the DPV responses at − 0.23 V were recorded. As shown in Table 2, the recoveries of these measurements ranged from 98.3% to 101.9% with RSD less than 5%, suggesting the high practicability in analyzing the real samples.

Conclusion

In this work, a novel electrochemical biosensor was designed for the sensitive detection of miRNA-21 based on a dual signal amplification strategy from both Bi_2O_3@Ti_3C_2 heterostructure and HCR. Although the HCR amplification strategy used to detect miRNA-21 is a relatively well-established method, it remains dynamic when used in conjunction with the exclusive structures such as Bi_2O_3@Ti_3C_2. The highly folded structure and superior active area of Bi_2O_3@Ti_3C_2 confer the ability to improve the molecular hybridization efficiency through collisions. The introduction of Au NPs further speeded up the electron transfer and biocompatibility of the Bi_2O_3@Ti_3C_2 nanocomposites. Most importantly, the detection of miRNA-21 in normal human serum verified the preferable practicability of the new sensor. The results achieved demonstrated that the proposed sensing platform shows great potential in early cancer diagnosis. In the coming work, synchronous multi-channel sensing of various miRNAs will be carried out based on such strategy to resolve the bottle-neck problem in synchronously sensing different miRNAs which are predicted to be comparable to other strategies for the detection of multiple targets in a single run of one serum sample.

Table 2 Determination of miRNA-21 added in normal human serum with the proposed biosensor ($n = 3$)

Sample	Added	Found	Recovery (%)	RSD (%)
1	0	/	/	/
2	100 pM	101.06 pM 98.43 pM 96.77 pM	98.7	1.79
3	1 pM	0.98 pM 0.93 pM 1.04 pM	98.3	4.57
4	10 fM	9.82 fM 10.34 fM 10.41 fM	101.9	2.58

Supplementary Information The online version contains supplementary material available at https://doi.org/10.1007/s00604-022-05624-8.

Funding This work was financially supported by the Natural Science Foundation of Shanghai (19ZR1434800), Shanghai Collaborative Innovation Center of Energy Therapy for Tumors, Clinical research project of Shanghai Municipal Health Commission (201940078), and Scientific research program of Shanghai Science and Technology Commission (21140903200). The authors greatly appreciated this support.

Declarations

Conflict of interest The authors declare no competing interests.

References

1. Yang X, Wu Y, Zhang B, Ni B (2018) Noncoding RNAs in multiple sclerosis. Clin Epigenet 10. https://doi.org/10.1186/s13148-018-0586-9
2. Li MX, Zhao W, Wang H, Li XL, Xu CH, Chen HY et al (2018) Dynamic single molecular rulers: toward quantitative detection of microRNA-21 in living cells. Anal Chem 90(24):14255–14259. https://doi.org/10.1021/acs.analchem.8b03322
3. He L, Hannon GJ (2004) MicroRNAs: small RNAs with a big role in gene regulation. Nat Rev Genet 5(7):522–531. https://doi.org/10.1038/nrg1379
4. Nassar FJ, Nasr R, Talhouk R (2017) MicroRNAs as biomarkers for early breast cancer diagnosis, prognosis and therapy prediction. Pharmacol Ther 172:34–49. https://doi.org/10.1016/j.pharmthera.2016.11.012
5. Shu XL, Fan CB, Long B, Zhou X, Wang Y (2016) The anticancer effects of cisplatin on hepatic cancer are associated with modulation of miRNA-21 and miRNA-122 expression. Eur Rev Med Pharmacol Sci 20(21):4459–4465
6. Herbst RS, Morgensztern D, Boshoff C (2018) The biology and management of non-small cell lung cancer. Nature 553(7689):446–454. https://doi.org/10.1038/nature25183
7. Li M, Wang Y, Liu X, Zhang Z, Wang L, Li Y (2020) miR-629 targets FOXO3 to promote cell apoptosis in gastric cancer. Exp Ther Med 19(1):294–300. https://doi.org/10.3892/etm.2019.8168
8. Li J, Wu Z, Zheng D, Sun Y, Wang S, Yan Y (2019) Bioinformatics analysis of the regulatory lncRNA-miRNA-mRNA network and drug prediction in patients with hypertrophic cardiomyopathy.

Mol Med Rep 20(1):549–558. https://doi.org/10.3892/mmr.2019.10289
9. Elemeery MN, Badr AN, Mohamed MA, Ghareeb DA (2017) Validation of a serum microRNA panel as biomarkers for early diagnosis of hepatocellular carcinoma post-hepatitis C infection in Egyptian patients. World J Gastroenterol 23(21):3864–3875. https://doi.org/10.3748/wjg.v23.i21.3864
10. Varallyay E, Burgyan J, Havelda Z (2007) Detection of microRNAs by Northern blot analyses using LNA probes. Methods 43(2):140–145. https://doi.org/10.1016/j.ymeth.2007.04.004
11. Lee W-H, Tsai M-J, Chang W-A, Wu L-Y, Wang H-Y, Chang K-F et al (2018) Deduction of novel genes potentially involved in hypoxic AC16 human cardiomyocytes using next-generation sequencing and bioinformatics approaches. Int J Mol Med 42(5):2489–2502. https://doi.org/10.3892/ijmm.2018.3851
12. Ahmed FE, Ahmed NC, Gouda MM, Vos PW, Bonnerup C (2018) RT-qPCR for fecal mature microRNA quantification and validation. Methods Mol Biol (Clifton, NJ) 1765:203–215. https://doi.org/10.1007/978-1-4939-7765-9_13
13. Zhuang Y, Huang F, Xu Q, Zhang M, Lou X, Xia F (2016) Facile, fast-responsive, and photostable imaging of telomerase activity in living cells with a fluorescence turn-on manner. Anal Chem 88(6):3289–3294. https://doi.org/10.1021/acs.analchem.5b04756
14. Xiao S, Wang X, Yang C, Jiang Y, Zhen S, Huang C et al (2022) Electrochemiluminescence resonance energy transfer system based on silver metal-organic frameworks as a double-amplified emitter for sensitive detection of miRNA-107. Anal Chem 94(2):1178–1186. https://doi.org/10.1021/acs.analchem.1c04368
15. Tian R, Zheng XW (2016) Sensitive colorimetric detection of microrna based on target catalyzed double-arm hairpin DNA assembling. Anal Sci 32(7):751–755
16. Liu X, Huang R, Su R, Qi W, Wang L, He Z (2014) Grafting hyaluronic acid onto gold surface to achieve low protein fouling in surface plasmon resonance biosensors. ACS Appl Mater Interfaces 6(15):13034–13042. https://doi.org/10.1021/am502921z
17. Cai W, Xie S, Tang Y, Chai Y, Yuan R, Zhang J (2017) A label-free electrochemical biosensor for microRNA detection based on catalytic hairpin assembly and in situ formation of molybdophosphate. Talanta 163:65–71. https://doi.org/10.1016/j.talanta.2016.10.086
18. Negahdary M, Angnes L (2022) Application of electrochemical biosensors for the detection of microRNAs (miRNAs) related to cancer. Coordination Chem Rev 464. https://doi.org/10.1016/j.ccr.2022.214565
19. Gao W, Dong H, Lei J, Ji H, Ju H (2011) Signal amplification of streptavidin–horseradish peroxidase functionalized carbon nanotubes for amperometric detection of attomolar DNA. Chem Commun 47(18). https://doi.org/10.1039/c1cc10840a
20. Ju H (2017) Signal amplification for highly sensitive immunosensing. J Anal Test 1(1). https://doi.org/10.1007/s41664-017-0008-6
21. Lei J, Ju H (2012) Signal amplification using functional nanomaterials for biosensing. Chem Soc Rev 41(6):2122–2134. https://doi.org/10.1039/c1cs15274b
22. Ju H (2012) Signal amplification for highly sensitive bioanalysis based on biosensors or biochips. J Biochips Tissue Chips 02(02). https://doi.org/10.4172/2153-0777.1000e114
23. Zhou QY, Ma RN, Hu CL, Sun F, Jia LP, Zhang W et al (2021) A novel ratiometric electrochemical biosensing strategy based on T7 exonuclease-assisted homogenous target recycling coupling hairpin assembly-triggered double-signal output for the multiple amplified detection of miRNA. Analyst 146(8):2705–2711. https://doi.org/10.1039/d1an00204j
24. Liu S, Yang Z, Chang Y, Chai Y, Yuan R (2018) An enzyme-free electrochemical biosensor combining target recycling with Fe3O4/CeO2@Au nanocatalysts for microRNA-21 detection. Biosens Bioelectron 119:170–175. https://doi.org/10.1016/j.bios.2018.08.006
25. Wang X, Liu G, Qi Y, Yuan Y, Gao J, Luo X et al (2019) Embedded Au nanoparticles-based ratiometric electrochemical sensing strategy for sensitive and reliable detection of copper ions. Anal Chem 91(18):12006–12013. https://doi.org/10.1021/acs.analchem.9b02945
26. Heiat M, Negahdary M (2019) Sensitive diagnosis of alpha-fetoprotein by a label free nanoaptasensor designed by modified Au electrode with spindle-shaped gold nanostructure. Microchem J 148:456–466. https://doi.org/10.1016/j.microc.2019.05.004
27. Duan F, Guo C, Hu M, Song Y, Wang M, He L et al (2020) Construction of the 0D/2D heterojunction of Ti3C2Tx MXene nanosheets and iron phthalocyanine quantum dots for the impedimetric aptasensing of microRNA-155. Sensors Actuators B Chem 310. https://doi.org/10.1016/j.snb.2020.127844
28. Feng A, Yu Y, Mi L, Yu Y, Song L (2018) Comparative study on electrosorptive behavior of NH4HF2-etched Ti3C2 and HF-etched Ti3C2 for capacitive deionization. Ionics 25(2):727–735. https://doi.org/10.1007/s11581-018-2787-9
29. Song H, Wang Y, Ling Z, Zu D, Li Z, Shen Y et al (2020) Enhanced photocatalytic degradation of perfluorooctanoic acid by Ti(3)C(2) MXene-derived heterojunction photocatalyst: Application of intercalation strategy in DESs. Sci Total Environ 746:141009. https://doi.org/10.1016/j.scitotenv.2020.141009
30. Đurđić S, Vukojević V, Vlahović F, Ognjanović M, Švorc Ľ, Kalcher K et al (2019) Application of bismuth (III) oxide decorated graphene nanoribbons for enzymatic glucose biosensing. J Electroanal Chem 850. https://doi.org/10.1016/j.jelechem.2019.113400
31. Liang L, Yang R, Han G, Feng Y, Zhao B, Zhang R et al (2020) Enhanced electromagnetic wave-absorbing performance of magnetic nanoparticles-anchored 2D Ti(3)C(2)T(x) MXene. ACS Appl Mater Interfaces 12(2):2644–2654. https://doi.org/10.1021/acsami.9b18504
32. Liu LZ, Song C, Zhang Z, Yang J, Zhou LL, Zhang X et al (2015) Ultrasensitive electrochemical detection of microRNA-21 combining layered nanostructure of oxidized single-walled carbon nanotubes and nanodiamonds by hybridization chain reaction. Biosens Bioelectron 70:351–357. https://doi.org/10.1016/j.bios.2015.03.051
33. Ge Z, Lin M, Wang P, Pei H, Yan J, Shi J et al (2014) Hybridization chain reaction amplification of microRNA detection with a tetrahedral DNA nanostructure-based electrochemical biosensor. Anal Chem 86(4):2124–2130. https://doi.org/10.1021/ac4037262
34. Lu J, Wu L, Hu Y, Wang S, Guo Z (2018) Ultrasensitive Faraday cage-type electrochemiluminescence assay for femtomolar miRNA-141 via graphene oxide and hybridization chain reaction-assisted cascade amplification. Biosens Bioelectron 109:13–19. https://doi.org/10.1016/j.bios.2018.02.062
35. Oishi M (2015) Enzyme-free and isothermal detection of microRNA based on click-chemical ligation-assisted hybridization coupled with hybridization chain reaction signal amplification. Anal Bioanal Chem 407(14):4165–4172. https://doi.org/10.1007/s00216-015-8629-y
36. Mahmoudian-Sani M-R, Asadi-Samani M (2020) Modulation of microRNAs by Euphorbia microsciadia Boiss in MDA-MB-231 cell line: new possibilities in breast cancer therapy. Recent Pat Anti-Cancer Drug Discovery 15(2):174–184. https://doi.org/10.2174/1574892815666200630102944
37. Guo J, Yuan C, Yan Q, Duan Q, Li X, Yi G (2018) An electrochemical biosensor for microRNA-196a detection based on cyclic enzymatic signal amplification and template-free DNA extension reaction with the adsorption of methylene blue. Biosens Bioelectron 105:103–108. https://doi.org/10.1016/j.bios.2018.01.036

38. Song Y, Wang MY, Qian Q, Xu J, Zhou QG, Lv SJ et al (2021) Trace miRNA assay based on DNA nanostructures formed by hybridization chain reaction and gold-nanoparticle tags. ChemElectroChem 8(15):2778–2782. https://doi.org/10.1002/celc.202100466
39. Tian W, Li P, He W, Liu C, Li Z (2019) Rolling circle extension-actuated loop-mediated isothermal amplification (RCA-LAMP) for ultrasensitive detection of microRNAs. Biosens Bioelectron 128:17–22. https://doi.org/10.1016/j.bios.2018.12.041
40. Dong J, Yang H, Zhao J, Wen L, He C, Hu Z et al (2022) Sandwich-type microRNA biosensor based on graphene oxide incorporated 3D-flower-like MoS(2) and AuNPs coupling with HRP enzyme signal amplification. Mikrochim Acta 189(1):49. https://doi.org/10.1007/s00604-021-05141-0
41. Guo WJ, Wu Z, Yang XY, Pang DW, Zhang ZL (2019) Ultrasensitive electrochemical detection of microRNA-21 with wide linear dynamic range based on dual signal amplification. Biosens Bioelectron 131:267–273. https://doi.org/10.1016/j.bios.2019.02.026
42. Bao J, Hou CJ, Zhao YA, Geng XT, Samalo M, Yang HS et al (2019) An enzyme-free sensitive electrochemical microRNA-16 biosensor by applying a multiple signal amplification strategy based on Au/PPy-rGO nanocomposite as a substrate. Talanta 196:329–336. https://doi.org/10.1016/j.talanta.2018.12.082
43. Zhou LL, Wang T, Bai Y, Li Y, Qiu JH, Yu W et al (2020) Dual-amplified strategy for ultrasensitive electrochemical biosensor based on click chemistry-mediated enzyme-assisted target recycling and functionalized fullerene nanoparticles in the detection of microRNA-141. Biosensors Bioelectronics 150. https://doi.org/10.1016/j.bios.2019.111964
44. Lu J, Wang J, Hu X, Gyimah E, Yakubu S, Wang K et al (2019) Electrochemical biosensor based on tetrahedral DNA nanostructures and G-quadruplex-hemin conformation for the ultrasensitive detection of microRNA-21 in serum. Anal Chem 91(11):7353–7359. https://doi.org/10.1021/acs.analchem.9b01133
45. Liang Z, Ou D, Sun D, Tong Y, Luo H, Chen Z (2019) Ultrasensitive biosensor for microRNA-155 using synergistically catalytic nanoprobe coupled with improved cascade strand displacement reaction. Biosens Bioelectron 146:111744. https://doi.org/10.1016/j.bios.2019.111744